Spectrally resolved neurophotonics: a case report of hemodynamics and vascular components in the mammalian brain

Kandice Tanner
Enrico D'Amico
University of Illinois at Urbana-Champaign
Department of Physics
Laboratory for Fluorescence Dynamics
Urbana, Illinois 61801

Amy Kaczmarowski
University of Illinois at Urbana-Champaign
Department of Psychology
Champaign, Illinois 61820

Shwayta Kukreti
University of Illinois at Urbana-Champaign
Department of Physics
Laboratory for Fluorescence Dynamics
Urbana, Illinois 61801

Joe Malpeli
University of Illinois at Urbana-Champaign
Department of Psychology
and Neuroscience Program
Champaign, Illinois 61820

William W. Mantulin
Enrico Gratton
University of Illinois at Urbana-Champaign
Department of Physics
Laboratory for Fluorescence Dynamics
Urbana, Illinois 61801
E-mail: Enrico@scs.uiuc.edu

Abstract. We developed a spectral technique that is independent of the light transport modality (diffusive or nondiffusive) to separate optical changes in scattering and absorption in the cat's brain due to the hemodynamic signal following visual stimulation. We observe changes in oxyhemoglobin and deoxyhemoglobin concentration signals during visual stimulation reminiscent of the functional magnetic resonance imaging (fMRI) blood oxygenation level dependence (BOLD) effect. Repeated measurements at different locations show that the observed changes are local rather than global. We also determine that there is an apparent large decrease in the water concentration and scattering coefficient during stimulation. We model the apparent change in water concentration on the separation of the optical signal from two tissue compartments. One opaque compartment is featureless (black), due to relatively large blood vessels. The other compartment is the rest of the tissue. When blood flow increases due to stimulation, the opaque compartment increases in volume, resulting in an overall decrease of tissue transmission. This increase in baseline absorption changes the apparent relative proportion of all tissue components. However, due to physiological effects, the deoxyhemoglobin is exchanged with oxyhemoglobin resulting in an overall increase in the oxyhemoglobin signal, which is the only component that shows an apparent increase during stimulation. © *2005 Society of Photo-Optical Instrumentation Engineers.* [DOI: 10.1117/1.2137291]

Keywords: photon migration; visual stimulation; brain activation; spectral approach.

1 Introduction

Optical techniques have been utilized to explore the hemodynamics of the visual cortex of the human brain[1] and that of animals.[2–4] Grinvald et al.,[5] Swindale et al.,[6] and Jancke et al.[7] have published several articles on the optical reflectance changes observed in the exposed brain surface of cats during visual stimulation. Here, we examine the visual cortex, specifically areas 17/18 of the cat using a spectral technique that enables noninvasive measurements through the skull. Specifically, we determine spectral changes due to changes in concentrations of tissue chromophores and scattering during visual stimulation. We show that the spectral technique is sensitive to changes due to neuronal activation by comparing the visual cortex with an area that lies outside the visual cortex; namely, the frontal lobes, where we expect little or no

signal change. This is the first study to employ a spectral technique to separate contributions from different tissue components with high temporal and spatial resolution. Several issues must be considered to interpret our results. Specifically, we consider the modality of light propagation in the tissue, the region of the brain explored by light, the physiological origin of the observed effects, and the potential and limitations of this spectral technique. We discuss our technical approach in the context of light transport in tissue to set the stage for the interpretation of the changes observed in the measured optical parameters. We show that different spectral components associated with known tissue chromophores can be identified and that the time course of the changes in spectral components can also be obtained. Several control measurements were done to validate that the observed effects result from the external visual stimulation.

In particular, we performed control trials without visual stimulation, with other conditions remaining the same. Brain

Address all correspondence to Enrico Gratton, Laboratory for Fluorescence Dynamics, Department of Physics, University of Illinois—Urbana-Champaign, 1110 W. Green St, Urbana, IL 61801. Tel: 217–244–5620. Fax: 217–244–7187. E-mail: enrico@scs.uiuc.edu

regions outside the cat's visual cortex were examined, during visual stimulation, to determine if the changes observed were localized to a specific region of the brain or were due to systemic changes in blood flow. The framework for the interpretation of the hemodynamic changes observed is based on the well-established BOLD effect (blood oxygenation level dependence response) from the functional magnetic resonance imaging (fMRI) literature. The BOLD effect is primarily due to neurovascular coupling between the part of the brain that is activated by a given task and the corresponding local increase in blood flow, following stimulation. This increase in flow causes a local decrease in the deoxyhemoglobin (HHb) content which is visible both in the MRI experiments and in the optical counterpart. In addition to changes in concentration of the HHb, the spectral method provides concomitant changes in concentration of other tissue chromophores such as oxyhemoglobin (O_2Hb) and water. Furthermore, the spectral approach that we developed provides changes in the scattering spectrum during brain activation. As a result of our studies, we have a comprehensive and novel description of changes occurring in specific brain regions due to neuronal activation. Our results confirm the general model of neurovascular coupling, and provide new information with regard to changes in the scattering spectrum and apparent changes in the local water concentration that require a new interpretation model. The time course of the optically detected BOLD effect shows unexpected features such as lack of sustainable blood flow increase and decrease of the amplitude of the effect as the task is repeated many times. These observations about fatigue in the cat brain will be discussed in a separate manuscript.

2 Light Transport in Tissues

Light transport in tissue is primarily governed by two processes; absorption and scattering. In the near-IR (NIR) region (650 to 1150 nm), in the so-called "therapeutic window," scattering is the dominant process for most tissues. For example, the reduced scattering coefficient $\mu_{s'}$ of the gray matter in the human brain ranges from 20 to 30 cm^{-1}, while the absorption coefficient μ_a is[8] about 0.25 cm^{-1}. In fleshy tissue, HHb, O_2Hb, and water are the main absorbing species[9] in the NIR. The large value of the reduced scattering coefficient of the brain enables the use of the diffusion approximation to the Boltzmann transport equation to describe the propagation of light and to quantify the absorption and scattering properties of the tissue when the distance traveled by the light between the source and the detector is[10–12] larger than 1 to 2 cm. However, for smaller distances (in the nondiffusive regime) a different approach must be employed to recover the optical parameters of tissues. Current diffuse optical techniques such as NIR spectroscopy (NIRS) use light at a few wavelengths chosen such that one can determine the concentrations of the HHb and O_2Hb. By using amplitude modulated light at moderately high frequencies (100 to 400 MHz), Gratton et al. showed that multidistance frequency-domain NIRS can be used as a noninvasive technique to study the hemodynamics of the muscle and brain.[13] It has been well documented[14] that the frequency-domain approach of light propagation in tissues provides high temporal resolution and a high SNR. In this paper, we explore a new spectral technique that employs a tungsten lamp source to study the hemodynamics of the tis-
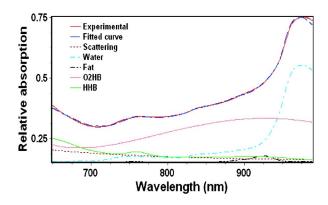

Fig. 1 Comparison of experimental and theoretical fit and the tissue chromophores used in the calculation.

sue, specifically the capillaries where the oxygen exchange takes place. We applied the spectral technique to detect changes in scattering and absorption in the visual cortex of a cat's brain due to the hemodynamic signal arising from neuronal activation evoked by visual stimulation. Note that we cannot apply the light transport formulation in the diffusion approximation for this experiment, because the anatomical structure of the cat's brain (namely, its small size) is such that there are insufficient scattering events when the light travels from the source fiber to the detector fiber. Hence, the photons are not fully randomized in direction before arriving at the detector. The spectral approach has been extensively used to study tissue spectral properties.[15–17] However, it has not been applied to study rapid changes in optical properties of brain tissue during visual stimulation. We are using a fast time acquisition (up to 200 spectra/s) to detect changes in cerebral hemodynamics.

3 Spectral Approach

In the NIR region, of the electromagnetic spectrum, the major chromophores found in tissue such as HHb, O_2Hb, fat, water, and cytochrome have well-defined absorption spectra (Fig. 1). To have all of the individual spectra on the same graph, they are not plotted on the same scale. HHb and O_2Hb are in units of mm^{-1} mM^{-1}, while water and fat are in units of inverse millimeters. The scattering spectrum in Fig. 1 follows the λ^n wavelength dependence with $n=4$. In the fit of the spectral changes the parameter n was variable.

In the spectral approach, we use a large number of wavelength points; hence, we can determine the absorbance of tissue components such as HHb, O_2Hb, fat, and water and their spectral shifts with high precision. Assuming that we know the spectrum of the individual tissue components, we can construct a linear combination of basis spectra to fit the overall tissue absorbance spectrum:

$$I = \text{scattering}(\lambda) + \text{water}(\lambda) + \text{fat}(\lambda) + O_2\text{Hb}(\lambda) + \text{HHb}(\lambda)$$

$$+ \text{cytochrome}(\lambda). \tag{1}$$

The coefficients of each term as well as the scattering power n are determined using a nonlinear least squares method. By knowing the coefficients used to fit the absolute spectrum, we estimate the fractional contribution of the individual compo-

nents in the measured tissue (Fig. 1). We apply the spectral approach to the differential spectrum obtained by subtracting the baseline period from the stimulation period. The differential changes are small, and we assume that the changes observed can be described by a linear combination of the basis components. However, for the application of the spectral approach in the differential measurements for tissue, the wavelength dependence of the scattering is allowed to vary and is not strictly fixed to a λ^{-4}, which is invalid for tissue. It was found using this technique that the actual dependence was $\lambda^{-0.4}$, as reported in the literature. Our system enables us to acquire spectra at a frequency of 200 Hz; hence, the relative tissue component contributions can be determined with high temporal resolution. Consequently, we can see the optical changes due to water, HHb, O_2Hb, and scattering as a function of time. These measurements can be used to potentially detect the BOLD response due to the neuronal activation. The spectral method separates scattering from absorption, as scattering has a characteristic spectral behavior different from any other spectral component. The spectral approach is different from the "frequency domain" method that exploits the time of flight in the diffusive regime to extract the scattering coefficient. One advantage of the spectral technique is that the spectral shape (including the scattering contribution) is independent of the light transport regime, i.e., it is applicable in both the diffusive and nondiffusive regime.

4 Methods—Cat Protocol

4.1 Preparation of the Cat

These experiments were performed on one adult female cat. All procedures were in accordance with U.S. Public Health Service Policy and protocols approved by the University of Illinois Institutional Animal Care and Use Committee. All surgery was performed aseptically and under general anesthesia. A goldplated ring was implanted under the conjunctiva of one eye to enable eye movements to be monitored using the double magnetic induction method.[18] The scalp and muscle overlying the calvarium were removed, and an aluminum fixture surrounding this area, bonded to the skull to provide support for a protective cap that was also used to immobilize the cat's head during the experiment. A mixture of clear acrylic cement and antibiotics ~1 mm thick was then placed in lieu of the removed tissue to provide a permanent protective barrier.[19] Metal tubes (15 gauge, thin-wall hypodermic tubing, with an inner diameter of 1.52 mm and an outer diameter of 1.83 mm), 7 mm in height, were then embedded in this mixture above the region corresponding to the visual cortex, area 17/18, and the frontal lobes, area 4. Figure 2 shows schematically the location of the metal tubes.[20] The tubes were in direct contact with the acrylic mixture above the bone. For simplicity, a grid system was implemented to indicate the position of each tube; this is used to identify the source and detector locations. The "a" row was located above the frontal lobes and each tube was numbered in sequence from 1 to 5. The "b" row was located in the parasagittally, roughly over the border between areas 17 and 18 of the visual cortex in the right hemisphere. The "c" row was located in a coronal plane that cut across the region of area 17 near the surface of the brain, as well as across the entire coronal extent of areas 18 and 19 of the visual cortex (Fig. 2). The intersection of the
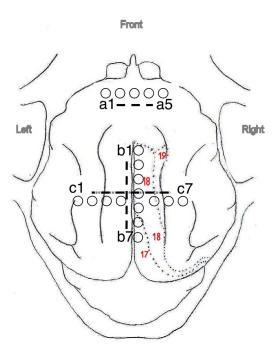

Fig. 2 Bird's eye view of placement of tubes on the calvarium of the cat with cortices labeled superimposed on a view of the dorsal surface of the cat brain.

"b" and "c" rows is roughly at the center of the representation of the area centralis. The distance between adjacent tubes was 2 mm, with the exception of c4 and c5, where the "c" row intersects the "b" row. The tubes served as holders for the source and detector optical fibers during our measurements.

4.2 Visual Stimulation and Behavioral Paradigm

The cat was positioned facing a rear projection screen subtending 60 deg horizontally and 50 deg vertically at a distance of 70 cm from the animal's eyes. The screen was illuminated uniformly at 0.021 cdm^{-2} with white light from an LCD projector. A computer controlled laser spot approximately 0.1 deg in diameter served as a fixation point on the center of the screen. Visual stimuli consisted of periodic flashes generated by white LED clusters that were superimposed on the screen raising the luminance to 2.020 cdm^{-2} during the flash.

The cat sat immobile in a bag with its head fixed to a rigid plate, tilted forward 5 deg with respect to the Horsley-Clark horizontal plane. During a trial, the cat was trained to focus on the fixation point regardless of the flashes, which had no behavioral significance. Generally, if the cat maintained this fixation (within ±7 deg) for 10 s, it was rewarded with food. The intertrial interval was 10 s. However, during data collection sessions, the cat was rewarded at the end of each trial regardless of its performance. For the purposes of this experiment there were two types of tasks, one in which the cat was visually stimulated (VS trial), and one where there was no visual stimulation (NVS).

1. VS trials consisted of 10 s of a repetitive sequence of 20 flashes where the flash was on for 250 ms and off for 250 ms, terminated by the reward followed by a 10-s intertrial interval.

2. NVS trials consisted of 10 s of no flashes, with delivery of the reward followed by a 10-s intertrial interval.

The trials were done with the NVS trials performed first (in blocks of 100) followed immediately by the VS trials (with minimum perturbation). This was achieved by toggling an external switch to activate the flash. Neither the cat nor the optical setup was disturbed in any way. The cat was monitored at all times with an IR-sensitive camera and light sources. The detector tubes were largely shielded from these light sources.

5 Experimental Procedure

5.1 Technical Aspects

Spectral measurements were performed using an Ocean Optics (830 Douglas Avenue, Dunedin, Florida) detector system consisting of a S2000 spectrometer, an ADC2000 PCI card and a tungsten lamp. The tungsten lamp gives a continuum spectrum following Planck's blackbody spectrum at a temperature of 3100 K. The PCI ADC2000 hardware interface between the spectrometer and the computer performed an analog to digital conversion at a sampling frequency of 2 MHZ at a 12-bit resolution, which enables spectral acquisition every 5 ms. Additionally, free-running operations and external trigger modes were available for synchronizing external events. The S2000 Ocean Optics is a miniature spectrometer with large spectral response (350 to 1100 nm) and good spectral resolution (0.3 to 10 nm). The spectral response is optimized for the NIR range. This was achieved by a combination of different accessories: a diffraction grating with a spectral response in the 550 to 1100-nm range (#4 in Ocean Optics catalog) and a long-pass filter to transmit wavelengths greater than 550 nm. These combined with the response of the CCD linear array detector, premounted on the spectrometer, gave us the required spectral range of analysis in the NIR region, 650 to 990 nm. The optical resolution and spectral response depend on the slit entrance on the spectrometer, groove density of the gratings, fiber optics diameter, and number of elements (pixels) of the detector.

Optimization of light detection through highly scattering tissues was achieved by using an entrance slit of 200 μm and a fiber optic core of 1000 μm. The grating had a groove density of 600 mm^{-1} and the CCD array has 2048 pixels. The combinations of these parameters gave us an optical resolution of 4 nm.

5.2 Data Acquisition

The cat was immobilized in a bag facing the screen with its head fixed to ensure minimal movement. The optical fibers were then positioned in the tubes on the cat's head. Any particular pair is indicated according to the labeling system used in Fig. 2. For example, a configuration of b4b6 refers to the placement of the source fiber in tube b4 and the detector fiber in tube b6.

The tip of each fiber was placed in direct contact with the acrylic which was roughly 1 to 2 mm above the cat's skull, and approximately 4 mm above the surface of the cat's brain. The cat's head was held rigidly fixed during the experiment, once the tubes were placed in the tubes; consequently their positions were stable and could be reproduced from session to session. The spectrometer was armed at the beginning of each trial by an external pulse coincident with a short auditory signal to indicate the start of the trial. Data acquisition and analysis were performed by the Elantest software (this program is available at ftp://www.lfd.uiuc.edu/lfd/egratton/elantest/), which communicated through the PCI ADC2000 card with the S2000 spectrometer. Synchronization of the data acquisition with the visual stimulation was achieved by an external Stanford Research (1290-D Reamwood Avenue, Sunnyvale, California) pulse generator (model DS345). The trigger and synchronization system provided the correct time signals to the Elantest software and the external trigger input port of the spectrometer. Communication with the software via the parallel port of the PC enabled the system for the start of data acquisition.

The spectrometer acquired spectra every 5 ms. First, a reference spectrum was taken under the condition of no trial, meaning that the cat observed the screen at its normal background level, as described in the previous section, but otherwise not performing the task. All differential measurements were calculated with respect to this initial spectrum. Equal blocks of data consisting of 100 trials were collected under different conditions. Data acquisition began with the beginning of each trial. The collection of spectra was synchronized with externally supplied pulses that were coincident with the onset of each flash in the VS condition (i.e., every 500 ms). The same timing was also provided for the NVS conditions. The spectrometer was armed at the start of each trial by an initial pulse and acquired a spectrum every 5 ms, giving a total of 95 spectra corresponding to 475 ms. The spectrometer then waited for the next trigger, which occurred 500 ms after the start of the trial. This cycle was repeated 16 times for a total of $\sim 16 \times 95$ spectra corresponding to about 8 s of the trial. No spectra were acquired during the final 2 s of the trial, the reward and the intertrial interval. Each spectrum had 2048 wavelength points. The data matrix was then saved and the sequence repeated 100 times. The procedure was repeated for different source-detector configurations. It was identical for NVS trials except that the pulses provided to synchronize the collection of spectra every 500 ms were not accompanied by flashes. The experiment was performed with minimum perturbation as the only change during the data acquisition was the activation of the flashes during the VS trials via an external computer.

5.3 Data Analysis

In this paper, we present the analysis of the hemodynamic signal. The analysis of the fast neuronal signal will be discussed in a separate manuscript. Data were collected for the first 8 s of each trial. However, every 475 ms, one spectrum was deleted due to the external synchronization of the system, as this spectrum had a different integration time (30 ms instead of 5 ms). This spectrum was disregarded, but the overall time axis was maintained correctly, i.e., the matrix had a gap of 30 ms every 500 ms. Since we were using this sequence only for slow signals, and the time axis was correct, this deletion had no influence on the final result. The remaining spectra were then folded across the 16 flash cycles and averaged over the desired number of trials. Folding was also done as a function of number of trials to see if there were any

differences in the signals observed due to physiological changes occurring across trials. A definitive spectral pattern and intensity pattern changes were observed in the raw data matrix. We performed spectral deconvolution and principal component analysis (PCA) on the raw, but folded data. From the PCA, it was determined that the minimum number of basis components required to correctly fit the differential spectrum was four: scattering, water, HHb, and O_2Hb. The spectrum was then separated into the weighted contributions of these individual species and their changes observed as a function of time. No assumptions were made with respect to the baseline hemoglobin concentrations as we only consider a differential spectrum. In representing the changes of the components as a function of time, only O_2Hb and HHb were plotted using the same scale. The scale of the changes in water component and that of the scattering component are arbitrary.

6 Results

For all of the different source-detector (S-D) configurations, data were processed as described in the previous section to detect both the changes due to the hemodynamic signal and to the fast (millisecond) neuronal signal. However, due to the volume of information that was obtained, only certain aspects of the hemodynamic signal are presented in this paper. First, we present maps of the raw data matrix after folding followed by the separation of this matrix into the weighted contributions of scattering, water, O_2Hb, and HHb as functions of time. The maps show the average change for all of the wavelengths as a function of time for the folded data. Finally a comparison of the optical BOLD effect seen as a function of S-D configuration is shown. Although we show results for only a few experiments, the results are highly reproducible for any given S-D combinations. For locations in the visual cortex, the optical BOLD effect is observed during visual stimulation and not seen in the absence of the stimulation. Similarly for S-D configurations located outside of the visual cortex (frontal lobes), the Optical BOLD effect was not observed for NVS or VS trials.

6.1 Raw Data

Maps displaying the raw data matrix of each S-D pair over the visual cortex, areas 17 and 18 show a significant change in the shorter wavelengths for the first 3 s of the visual stimulation [Fig. 3(a) and 3(c)]. The data matrix for the control configuration that was positioned over the frontal lobes, where we did not anticipate any changes, remains relatively constant during the same activation period [Fig. 3(e)]. For all of the configurations during NVS trials, the changes in wavelengths as a function of time were also minimal [Fig. 3(b), 3(d), and 3(f)].

6.2 Spectral Deconvolution

The raw data matrix was decomposed for each time bin (linked to trial length) using four spectral components: O_2Hb, HHb, water, and scattering. Figures 4(a)–4(f) show three different S-D locations for VS and NVS trials, one from the parasagittal row of tubes over the area 17/18 border [b4b6; Figs. 4(a) and 4(b)], one roughly in a coronal plane over areas 17 and 18 [b4c6; Figs. 4(c) and 4(d)], and one over the frontal lobes [a2a4; Figs. 4(e) and 4(f)]. There is an optically detected

BOLD effect due to the activation of the visual cortex in which the O_2Hb starts to increase after 1 to 2.5 s after visual stimulation. This delay is dependent on the area investigated. Differences in the values and time courses of the signals due to changes in O_2Hb and HHb are detected between regions in the visual cortex which differ by about 2 mm. Additionally, significant changes are seen due to scattering and water. The change due to scattering also has a different time course with respect to the other components. For S-D configurations that correspond to areas in the visual cortex, a maximum decrease (trough) in scattering is seen at roughly the same time as the O_2Hb reaches a maximum in the optical BOLD effect during VS trials. The water component is seen to decrease at the onset of stimulation and tracks the HHb changes with some time delay [Figs. 4(a) and 4(b)]. Control experiments [Figs. 4(e) and 4(f)] show that there are no major changes in the O_2Hb and HHb (BOLD effect) that track with the visual stimuli for the S-D pair located over the frontal lobes, and the contributions from these components are one order of magnitude smaller than the signal obtained from the VS trials [Figs. 4(a) and 4(c)]. The signals due to the changes in water and scattering are of the same order of magnitude, but they do not appear to be correlated to visual stimulation. In addition, control experiments show minimal signal changes in the absence of visual stimulation [Figs. 4(b), 4(d), and 4(f)].

6.3 Optical BOLD Effect as a Function of S-D Locations

Figures 5(a) and 5(b) show the optically detected BOLD effect for several S-D locations, two parallel to the 17/18 border (b4b6, b3b5), and one S-D pair located over the frontal lobes (a2a4), and three that roughly straddled this border orthogonally (b4c6, b4c5, and c5b5), respectively. The signals for the two S-D configurations parallel to the 17/18 border show similar temporal behavior. However, for the configuration b4b6 the amplitude of the signal is much larger (about a factor of 4) than for any other configuration. For the orthogonal S-D pairs, it was observed that the amplitude of the signal due to the optical BOLD effect was approximately the same. However, there were different delays among the different pairs. In one configuration, b4c6, an initial dip is seen lasting for ~2 s. The initial dip was not observed at all locations, indicating that its magnitude is not constant everywhere.

7 Discussion

This work is the first to determine changes of the spectral components in the mammalian (cat) brain due to external visual stimuli. Previous work focused on the determination of the reflectance signal in the near-IR with the purpose of imaging columnar neuronal organization,[21] and the optically detected BOLD effect was not determined in those studies. Furthermore, the fast dynamics were obtained using long-integration, high-sensitivity cameras in which the acquisition was triggered at different times after visual stimulation rather than utilizing rapid spectral acquisition, which was synchronous with the visual stimulation as in the present approach. The spatial resolution that is obtained with our instrument is of the order of millimeters, which when compared to that obtained using multidistance NIRS in human subjects (centimeters) still gives us a relatively high spatial resolution. One
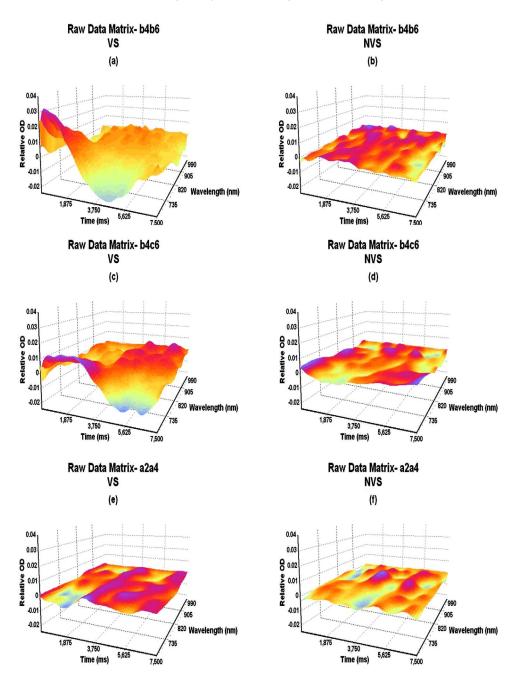
Fig. 3 Raw data matrix indicating source and detector location and trial type: (a) b4b6 VS, (b) b4b6 NVS, (c) b4c6 VS, (d) b4c6 NVS, (e) a2a4 VS, and (f) a2a4 NVS.

concern is that the radiation emitted by the tungsten lamp will be unstable as it is temperature dependent. However, before any analysis was done, the data was block averaged and folded across trials as is standard in similar studies. Hence, any random fluctuations that are present would be removed before the spectral deconvolution is performed. We have observed changes in the O_2Hb and HHb signals during visual stimulation reminiscent of the fMRI BOLD effect. The origin of the BOLD effect is attributed to an increase in blood flow following neuronal activity in one part of the brain. This causes a decrease of the HHb level because HHb is washed out. In the fMRI signal, only the decrease of the HHb concentration is measured, whereas with the optical technique,

we have access to both O_2Hb and HHb. Upon visual stimulation, we can clearly see the decrease in the HHb and the quasisimultaneous increase in the O_2Hb. Careful examination of the data in Figs. 5(a) and 5(b) shows that there is a delay between the two signals. A similar delay between the increase of the O_2Hb and decrease of HHB was also observed in optical experiments in humans and was attributed to oxygen consumption.[22,23] A striking feature of our experiments is that the optical BOLD effect starts to decrease after a few seconds [Fig. 5(a)], although the stimulation continued throughout the trial.
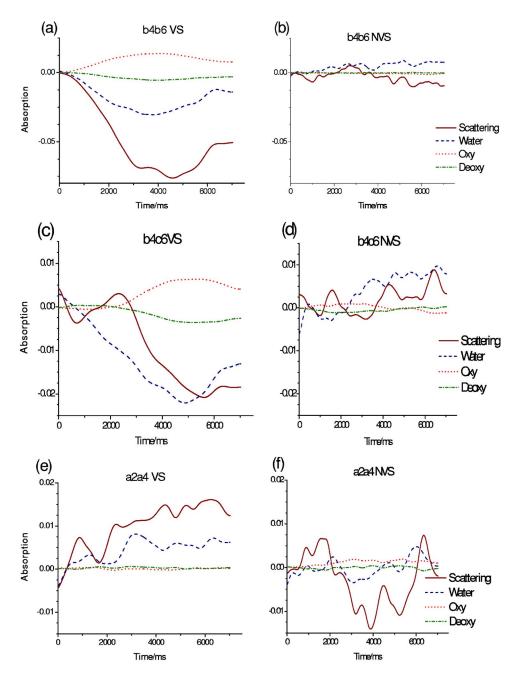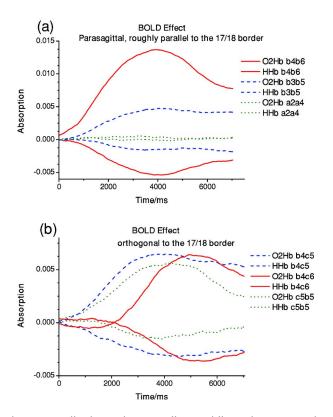
Fig. 4 Spectral deconvolution, O_2Hb, and HHb: (a) b4b6 VS (b), b4b6 NVS, (c) b4b6 VS, (d) b4b6 NVS, (e) a2a4 VS, and (f) a2a4 NVS.

Another novel outcome of these experiments is that the water signal, as well as the scattering signal, changes during stimulation. The changes in the water component are quite surprising, since we expect no net change of the tissue water content during the short time of visual stimulation. For the water content in the tissue to change rapidly (in seconds), the water should be replaced by something else, which is not plausible. To explain the decrease of the water content during the optical BOLD effect we must consider the origin of the optical signal in the tissue. The tissue is highly heterogeneous from both the physiological and the optical points of view. There are tissue regions that are optically opaque, such as relatively large blood vessels. If, as we expect, these vessels change diameter to accommodate an increase of blood flow

following neuronal stimulation, then this opaque optical compartment will increase. The net effect of the increase in the opaque compartment results in an effective decrease of all the spectral components, including the O_2Hb and HHb. However, these tissue chromophores undergo additional physiological changes due to the exchange of O_2 and CO_2 in the tissue, which results in a net increase of the O_2Hb signal (washout effect). We propose that this optical effect caused by the presence of the opaque blood vessels is at the origin of the apparent decrease of the water component. Following this reasoning, the water component could be used to assess the extent of vasodilation due to stimulation. With regard to the scattering signal, it should also decrease due to this optical effect. How-

(a)

(b)

Fig. 5 Optically detected BOLD effect at different locations in the visual cortex. For each curve, positive line indicates O$_2$Hb and negative line indicates HHb (a) for parasagittal S-D pairs, which were roughly parallel to the 17/18 border, and (b) for S-D pairs roughly orthogonal to the 17/18 border.

ever, there are also changes in the size of the microcapillaries, larger blood vessels, and possible changes at the cellular and subcellular levels. Therefore, the scattering signal will not necessarily track the water signal.

All data presented in Figs. 5(a) and 5(b) refer to only the first 10 trials of a series of 100 trials. As the trials continued, there was a gradual change of the shape of the optical BOLD effect. This fatigue effect will be discussed in a separate manuscript.

We observed that the optical BOLD effect is strongly dependent on the location in the visual cortex. Locations 2 mm apart gave significant differences both in the amplitude and in the time course of the signals.

We observed several differences between the optical BOLD effect for the cat, when compared with similar experiments in humans. It is premature to discuss the differences, when only one animal has been studied. Furthermore, we cannot state unequivocally that these results are "cat invariant." However, additional cats are being trained to repeat the experiments, and to assess if there are differences among individual animals. Certainly the size of the cat's brain could generate hemodynamic responses that differ from those in humans.

One consideration for this discussion is whether or not the spectral approach could be extended to studies of the human brain. First, the size of the skull will bring the regime of light propagation into the diffusive regime. However, the spectral approach is independent of the modality of light propagation.

Two factors must be considered for the application of this spectral approach in humans. First, with the present experimental apparatus, the SNR is insufficient to observe the dynamic changes of the tissue chromophores at the distance of centimeters. For the slow hemodynamic signal, using more sensitive detectors and more efficient monochromators, we should have enough light for an accurate determination of spectral components. Second, for the fast signal due to neuronal activation, where a very short integration time is required, the amount of light necessary could be critical. Hence, additional work is required for the improvement of the technical aspects of this work.

In summary, we developed a technique that is independent of the light modality (diffusive or nondiffusive), where a broadband spectral approach is used to determine the individual NIR spectrum of tissue components. For the application in a mammalian brain, we have examined the behavior of the scattering, O$_2$Hb and HHb (BOLD effect) simultaneously with other tissue components such as water content. The technique has proven to have a high temporal and spatial resolution to adequately determine the localized hemodynamics. The behavior of water during stimulation has not been discussed in previous literature. Our proposed model satisfactorily accounts for the apparent change in the water content, which can be used to better qualify the role of water in vascular dynamics.

References

1. M. Wolf, U. Wolf, V. Toronov, A. Michalos, L. A. Paunescu, J. H. Choi, and E. Gratton, "Different time evolution of oxyhemoglobin and deoxyhemoglobin concentration changes in the visual and motor cortices during functional stimulation: a near-infrared spectroscopy study," *Neuroimage* **16**, 704–712 (2002).
2. J. Mayhew, D. Johnston, J. Berwick, M. Jones, P. Coffey, and Y. Zheng, "Spectroscopic analysis of neural activity in brain: increased oxygen consumption following activation of barrel cortex," *Neuroimage* **12**, 664–675 (2000).
3. R. Frostig, E. Lieke, D. Ts'o, and A. Grinvald, "Cortical functional architecture and local coupling between neuronal activity and microcirculation revealed by in vivo high resolution optical imaging of intrinsic signals," *Proc. Natl. Acad. Sci. U.S.A.* **87**, 6082–6086 (1990).
4. D. Shoham, M. Hubener, A. Grinvald, and T. Bonhoeffer, "Spatio-temporal frequency domains and their relation to cytochrome oxidase staining in cat visual cortex," *Nature (London)* **385**, 529–533 (1997).
5. A. Grinvald, E. Lieke, R. D. Frostig, C. D. Gilbert, and T. N. Wiesel, "Functional architecture of cortex revealed by optical imaging of intrinsic signals," *Nature (London)* **324**, 361–364 (1986).
6. N. V. Swindale, D. Shoham, A. Grinvald, T. Bonhoeffer, and M. Hübener, "Visual cortex maps are optimized for uniform coverage," *Nat. Neurosci.* **3**, 822–826 (2000).
7. D. Jancke, F. Chavane, S. Naaman, and A. Grinvald, "Imaging cortical correlates of illusion in early visual cortex," *Nature (London)* **428**, 423–426 (2004).
8. P. Van der Zee, M. Essenpreis, and D. T. Delpy, "Optical properties of brain tissue," *Proc. SPIE* **1888**, 454–465 (1993).
9. V. Venugopalan, "Tutorial in tissue optics," in *Proc. Optical Society of America BIOMED Topical Meeting* (2004).
10. A. Ishimaru, *Wave Propagation and Scattering in Random Media,*

Vol. 1, Academic Press, New York (1978).

11. M. S. Patterson, B. Chance, and B. C. Wilson, "Time-resolved reflectance and transmittance for the non-invasive measurement of tissue optical properties," *Appl. Opt.* **28**, 231–236 (1989).

12. J. B. Fishkin and E. Gratton, "Propagation of photon density waves in strongly scattering media containing an absorbing semi-infinite plane bounded by a straight edge," *J. Opt. Soc. Am. A* **10**, 127–140 (1993).

13. E. Gratton, S. Fantini, M. A. Franceschini, G. Gratton, and M. Fabiani, "Measurements of scattering and absorption changes in muscle and brain," *Philos. Trans. R. Soc. London, Ser. B* **352**, 727–735 (1997).

14. M. Wolf, M. A. Franceschini, L. A. Paunescu, V. Toronov, A. Michalos, U. Wolf, E. Gratton, and S. Fantini, "Absolute frequency-domain pulse oximetry of the brain: methodology and measurements," *Adv. Exp. Med. Biol.* **530**, 61–73 (2003).

15. J. Mayhew, D. Johnston, J. Berwick, M. Jones, P. Coffey, and Y. Zheng, "Spectroscopic analysis of neural activity in brain: Increased oxygen consumption following activation of barrel cortex," *Neuroimage* **12**, 664–675 (2000).

16. E. Shtoyerman, A. Arieli, H. Slovin, I. Vanzetta, and A. Grinvald, "Long term optical imaging and spectroscopy reveal mechanisms underlying the intrinsic signal and stability of cortical maps in V1 of behaving monkeys," *J. Neurosci.* **20**, 8111–8121 (2000).

17. S. Schuett, T. Bonhoeffer, and M. Huebner, "Mapping retinotopic structure in mouse visual cortex with optical imaging," *J. Neurosci.* **22**, 6549–6559 (2002).

18. H. Cui and J. Malpeli, "Activity in the parabigeminal nucleus during eye movements directed at moving and stationary targets," *J. Neurophysiol.* **89**, 3128–3142 (2003).

19. A. Tate and J. Malpeli, "Effects of focal inactivation of dorsal or ventral layers of the lateral geniculate nucleus on cat's ability to see and fixate small targets," *J. Neurophysiol.* **80**, 2206–2209 (1998).

20. F. Reinoso-Suarez, *Topographischer Hirnatlas der Katze, fur Experimental-Physiologische Unstersuchungen*, Vol. 4 E. Merck AG, Darmstadt (1961).

21. A. Shmuel and A. Grinvald, "Functional organization for direction of motion and its relationship to orientation maps in cat area 18," *J. Neurosci.* **16**, 6945–6964 (1996).

22. V. Toronov, A. Webb, J. H. Choi, M. Wolf, L. Safonova, U. Wolf, and E. Gratton, "Study of local cerebral hemodynamic fluctuations by simultaneous frequency-domain near-infrared spectroscopy and fMRI," *Opt. Express* **9**, 417–427 (2001).

23. S. Ogawa, R. S. Menon, S. G. Kim, and K. Ugurbil, "On the characteristics of functional magnetic resonance imaging of the brain," *Annu. Rev. Biophys. Biomol. Struct.* **27**, 447–474 (1998).